Industrial demonstration of indirect mineral carbonation in the cement and concrete sector

Journal Article

Author(s):
Meijssen, Mattheus; Marinello, Lena; di Bella, Carmelo; Gasós, Antonio; Mazzotti, Marco

Publication date:
2023-10

Permanent link:
https://doi.org/https://doi.org/10.3929/ethz-b-000631073

Originally published in:
Journal of Environmental Chemical Engineering 11(5), https://doi.org/10.1016/j.jece.2023.110900

Journal of Environmental Chemical Engineering 11 (2023) 110900

Contents lists available at ScienceDirect

Journal of Environmental Chemical Engineering

journal homepage: www.elsevier.com/locate/jece

Industrial demonstration of indirect mineral carbonation in the cement and concrete sector

Mattheus Meijssen [a], Lena Marinello [a], Carmelo di Bella [b], Antonio Gasós [a], Marco Mazzotti [a,*]

[a] Institute of Energy and Process Engineering, ETH Zurich, 8092 Zurich, Switzerland
[b] Jura-Cement-Fabriken AG, Talstrasse 13, 5013 Wildegg, Switzerland

ARTICLE INFO

Editor: Dong-Yeun Koh

Keywords:
CCUS
CO2 capture
Negative emmissions
Mineral carbonation
concrete

ABSTRACT

This paper reports on the successful construction, commissioning and operation of a mobile indirect mineral carbonation (IMC) pilot plant in the concrete sector. This work confirms the technical feasibility of IMC at large scale, while producing precipitated calcium carbonate (PCC) and leached recycled concrete aggregate (RCA) as useful products. The plant is capable of handling industrial flue gas or pure CO_2 as carbon feedstock, while processing around 80 kg/h of RCA as calcium feedstock, and storing around 0.9 kg/hr of CO_2. Good recyclability of the aqueous ammonium nitrate mother liquor is suggested, although small changes occurred over time, with only small effects on the operation. Importantly, some $CaCO_3$ precipitates in the dissolution reactor, especially at high CO_2 feed rates; this does not decrease the CO_2 storage rate, but it reduces the PCC production rate. The plant may be operated at a variety of operating conditions and it responds to them as expected from thermodynamic considerations. Similarly, the trade-offs in terms of performance parameters also change as expected. The observed calcium extraction efficiency is rather low due to the thermodynamic nature of the batch dissolution step. Also, the ammonium nitrate losses are rather high due to the plant not having a solvent recovery step integrated. Potentially alternative reactor concepts for the dissolution section can improve the calcium extraction efficiency while including a washing step, thus alleviating the main limitation. Material tests with the products of the process suggest that leached RCA is as good as, or even better than fresh RCA for use as aggregate in concrete; ground PCC performs similar as ground limestone in cement, however it is not the most attractive use of fine PCC, as higher value applications exist. Although improvements to the plant design are necessary to make the process economically and environmentally viable, this work represents an important steppingstone towards industrial implementation of IMC, and confirms its technical feasibility in the concrete sector.

1. Introduction

Concrete, made from cement, aggregate and water, is the most utilized construction material in the world with a global annual consumption of around 25 Gt [1,2]. Cement accounts for only ~ 10 wt % of concrete [3], yet it is responsible for ~ 70 % of its green house gas (GHG) emissions [3,4]. The estimated footprint of the most commonly used cements is between 600 and 990 kg CO_2 per tonne cement [5–7]. The production of cement starts by blending limestone, clay and minor amounts of additives. This mixture is referred to as the raw meal and mainly contains the compounds $CaCO_3$ (~ 77 wt %), SiO_2 (~ 14 wt %), and small amounts of other minerals [8]. The raw meal is heated to approximately 850˚C, where $CaCO_3$ decomposes into CaO and CO_2, through the process called calcination. Thereafter, the mixture is further heated in a rotating kiln to 1450˚C, thus iniatiting sintering and formation of the cementitious phases. The main cementitious phases in this intermediate material, referred to as clinker, are alite (Ca_3SiO_5) and belite (Ca_2SiO_4), and a few others, depending on the raw meal composition [9], though to a lesser extend. Finally the clinker is ground and mixed with small amounts of gypsum, which controls hydration reactions of the cementitious phases; this final product is cement [3]. Around two thirds of the generated CO_2 stem from the calcination chemistry itself, one third originate from the fuel used for heating, and a small fraction from other activities [8]; in a future net-zero world all these emissions will have to be adversed [10,11].

Currently several pathways are under investigation [3,12–14] of which carbon capture and storage (CCS) and carbon capture and utilization (CCU) are the most relevant and the best scalable pathways. An alternative, smaller scale solution is found in ex-situ mineral

* Corresponding author.
E-mail address: marco.mazzotti@ipe.mavt.ethz.ch (M. Mazzotti).

https://doi.org/10.1016/j.jece.2023.110900
Received 15 June 2023; Received in revised form 28 August 2023; Accepted 29 August 2023
Available online 1 September 2023

Latin symbols

n_i	solid concentration of species *i* mol/kg
$\hat{c}_i$	apparent liquid concentration of component *i* mol/kg
c_i	liquid concentration of species *i* mol/kg
$\hat{n}_i$	apparent solid concentration of component *i* mol/kg
c^*_{CH}	solubility concentration of calcium hydroxide mol/kg
t	time hour
a_i	activity of species *i* mol/kg
S_i	saturation of species *i* –
T	temperature ˚C
P_{CO2}	partial pressure of CO_2
C/S	calcium over silica ratio in CSH –
S_i	saturation of species *i* –
y_{CH}	fraction of the extractable calcium as CH –
S/L	solids mass per liquid mass in the dissolution reactor –
Q	liquid flow rate
W	solvent retention in the RCA
f	relative gas flowrate mol/l
F	gas flow rate mol/h
s_{CO2}	CO_2 storage rate mol/h
p_{CC}	PCC production rate mol/h
u_{AN}	ammonium nitrate utilization –

Greek symbols

τ_j	residence time in reactor *j* hour
ψ	ratio of carbon and calcium in solution –
η_{Ca}	calcium efficiency –
η_C	carbon efficiency –

Indices

i	species or component
j	reactor

Acronyms

PSD	Particle Size Distribution
CH	Calcium Hydroxide
CSH	Calcium Silicate Hydrate
AN	Ammonium Nitrate
RCA	Recycled Concrete Aggregate
SCM	Supplementary Cementitious Material
GHG	Green House Gas
CCS	Carbon Capture and Storage
CCU	Carbon Capture and Utilization
CCUS	Carbon Capture and Utilization
PCC	Precipitated Calcium Carbonate
AN	Ammonium Nitrate
XRD	X-Ray Diffraction
IMC	Indirect Mineral Carbonation

carbonation [15,16], whereby CO_2 is bound to alkaline species in waste streams, i.e., magnesium or calcium, to form stable carbonates. This stores CO_2 permanently in the form of useful materials for the (road-) construction industry or for potentially other sectors[17]. As this pathway both effectively utilizes and permanently stores CO_2, it may be referred to as carbon capture, utilization and storage (CCUS). Several technologies within the space of mineral carbonation have been developed [16,18,19], and some have been commercialized [20–22].

A promising novel technology in this space is the so-called indirect mineral carbonation (IMC) [23,24]; a basic flow-scheme of this process applied in the concrete and cement sector is shown in Fig. 1. In the first step of IMC, calcium is extracted from recycled concrete aggregate (RCA) in the dissolution reactor using a weak acidic solution, after which the solution is filtered and a first product, i.e., leached RCA,

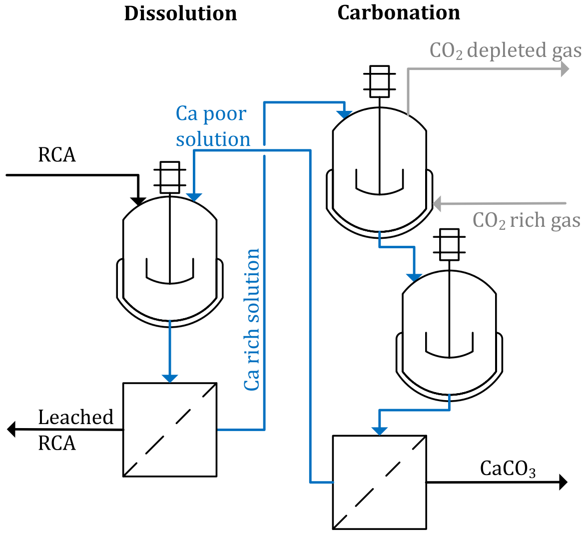

Fig. 1. A simplified flow-scheme of indirect mineral carbonation with the batch dissolution section on the left and a continuous 2-stage carbonation section on the right.

leaves the plant; this is referred to as the dissolution section of the process and is operated batch-wise. The clear solution, rich in calcium, is then brought into contact with a CO_2-rich gas in the absorption reactor, where CO_2 is absorbed, thus causing pure $CaCO_3$ to precipitate. The slurry is then fed to a growth reactor, where the suspension is given the time to reach thermodynamic equilibrium (this growth step is in principle optional). Finally, the slurry is filtered and the second product, i.e., precipitated $CaCO_3$ (PCC), leaves the plant, while the mother liquor, calcium-lean, is fed back to the dissolution reactor. The absorption reactor, the optional growth reactor, and the following filtration step are referred to as the carbonation section, which is operated in a continuous mode. The two products of this process, leached RCA and PCC, can be re-used in the manufacturing of cement and/or concrete, thereby storing CO_2 permanently [8] and reducing its environmental impact. In earlier works the individual process steps have been investigated at lab scale [25–27]. However, not much effort has been devoted to investigating the entire process and the usability of its products in the concrete and cement sector, let alone at an industrially relevant scale. In order to progress the technology towards commercialization, the process has to be investigated outside of a laboratory environment, i.e., at a larger scale using relevant unit operations in an industrial environment.

This is the ultimate goal of this work, whose focus is the construction and operation of a mobile pilot scale facility, capable of handling typical flue gas as well as pure CO_2 as carbon feedstock, and 0–4 mm RCA as calcium feedstock. The two types of gases are selected to assess the following: either (1) operation at a cement site, where flue gas with roughly 20 % CO_2 is available but the RCA has to be transported to, or (2) operation at a concrete site, where the RCA is available, but pure CO_2 has to be transported to. The RCA size fraction of 0–4 mm is selected as it is an available, low value waste stream, which has great potential for IMC due to its size and relatively high calcium content [25,28].

The paper is divided into four sections: First, in Section 2 the process-relevant theory and thermodynamic framework are presented. Then, Section 3 describes the mobile pilot unit, its equipment, the materials used, and the methodologies applied during the experimental campaign. After that the results of the experiments are presented and discussed in Section 4, which is followed by the conclusions in Section 5.

2. Thermodynamic framework

The process consists of three physico-chemical steps: (i) leaching of calcium in the dissolution reactor, (ii) absorption of CO_2 in the absorber, and (iii) precipitation of $CaCO_3$ in both the absorber and the growth reactor. Calcium, carbon and ammonium nitrate speciate in the solution, the species formed can be assumed to be in chemical equilibrium with one-another to understand how the process operates; the ions and molecules present in such a solution are listed in Table 1.

Their concentrations, c_i, and activities, a_i, are solely a function of the total calcium content, $\widehat{c}_{Ca}$, and of the total carbon content, $\widehat{c}_C$ (assuming no impurities, constant ammonium nitrate concentration, and constant temperature; for details on the speciation reactions, see appendix). It is the concentration or the activity of specific species that determine the driving forces for the three physico-chemical steps in the process, hence, the steps can be illustrated in a phase diagram having as coordinates $\widehat{c}_{Ca}$ and $\widehat{c}_C$, as shown in Fig. 2 for an ammonium nitrate concentration, $\widehat{c}_{AN} = 0.25$ M, a solid loading, $S/L = 0.2$, using RCA I as feed material (see Section 3.1.2), and pure CO_2 (the details of Fig. 2 are discussed below).

2.1. Dissolution

In the dissolution reactor, the two calcium containing phases of the RCA that dissolve are calcium hydroxide (CH) and calcium silicate hydrate (CSH). The total amount of dissolvable calcium in fresh RCA is denoted $\widehat{n}_{Ca,0}$, whereas the fraction of dissolvable calcium as CH, y_{CH}, is typically around 40 % [25], as assumed throughout this work. The dissolution reactions occurring when the solid phases are contacted with an (acidic) aqueous solution can be written as [29–32]:

$$Ca(OH)_2(s) \leftrightarrow Ca^{2+} + 2OH^- \tag{1a}$$

$$xCaO * SiO_2{\cdot}zH_2O(s) \longrightarrow (x-\delta)CaO * SiO_2{\cdot}(z-\delta)H_2O(s) + \delta Ca^{2+} + 2\delta OH^- \tag{1b}$$

here x refers to the calcium to silicate ratio in the CSH or as often used in literature, the C/S ratio. The dissolution of CSH is referred to as incongruent dissolution of a solid solution; calcium hydroxide is leached into the liquid phase whereby the solid phase, transitions into a de-calcified solid phase, with lower calcium hydroxide content.

The equilibrium concentration for calcium extraction from RCA in a batch reactor, $\widehat{c}_{Ca,eq}$, is given by the following relationship, as demonstrated earlier [25]:

$$\widehat{c}_{Ca,eq} = \begin{cases} \widehat{c}*_{CH} & \text{if } y_{CH}S/_L\ \widehat{n}_{Ca,corr} > \widehat{c}*_{CH} \\ \widehat{c}*_{CH}\dfrac{S\ \widehat{n}_{Ca,corr}}{S\ y_{CH}\ \widehat{n}_{Ca,corr}(1-y_{CH}) + L\widehat{c}_{CH}*} & \text{if } y_{CH}S/_L\ \widehat{n}_{Ca,corr} \le \widehat{c}*_{CH} \end{cases} \tag{2}$$

Here $\widehat{c}*_{CH}$ is the solubility of CH, which is a function of $\widehat{c}_C$ (see appendix for details), and $\widehat{n}_{Ca,corr}$ is the corrected amount of dissolvable calcium in the solids at the start of dissolution (the correction is derived and discussed in Section 2.3). Fig. 2 shows $\widehat{c}_{Ca,eq}$ as a green solid line; the dotted arrow, indicated with "dissolution", represents the change of composition in the reactor. The residence time in the dissolution reactor, τ_D, will determine how close to the equilibrium the final composition of the solution is. Typically at a residence time, $\tau_D = 30$ min, with $S/L = 0.2$, a level of about $0.5\widehat{c}_{Ca,eq}$ is reached; this is represented in Fig. 2 by the green cross.

Table 1
The ions and molecules in the solution due to the speciation of calcium, carbon and ammonium nitrate in water.

H^+	OH^-	Ca^{2+}	NH_4^+	$NH_3(aq)$	NO_3^-	$CaOH^+$
$CO_2(aq)$	HCO_3^-	CO_3^{2-}	$CaHCO_3^+$	$CaCO_3(aq)$	$CaNO_3^+$	NH_2COO^-

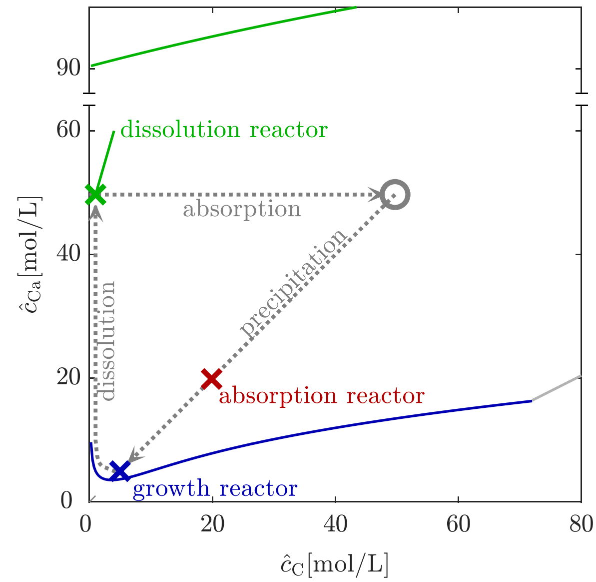

Fig. 2. Illustration of the thermodynamic equilibria (the solid lines) for the three physico-chemical steps in the process (the dotted lines), and the compositions in the reactors (the crosses). Furthermore, $\widehat{c}_{AN} = 0.25$ M, $T = 25$°C, $S/L = 0.2$, typical RCA is assumed, and pure CO_2 is used as gas feed.

2.2. Absorption and precipitation

After filtration, which removes any calcium remaining in the solid particles, the solution is transferred to the absorber where it is contacted with gaseous CO_2, which absorbs. Assuming equilibrium at the gas-liquid interface is given by Henry's law, the driving force for absorption is determined by the difference between $c_{CO_2(aq)}$ at the gas-liquid interface and that of the bulk solution. The grey solid line in Fig. 2 represents the equilibrium composition of the solution at the gas-liquid interface for pure gaseous CO_2 at ambient pressure, i.e.:

$$P_{CO_2} = H_{CO_2}(T)x_{CO_2(aq)} \tag{3}$$

Where $H_{CO_2}(T)$ is the Henry's constant for CO_2 in water, p_{CO_2} is the CO_2 partial pressure of the gas, and $x_{CO_2(aq)}$ is the corresponding mole fraction of CO_2 in the solution which is given by $c_{CO_2(aq)}/c_{tot}$. The grey dotted arrow in Fig. 2, labelled "absorption", represents the change of the composition assuming an amount of CO_2 absorbed in the bulk solution, stochiometric with respect to the calcium fed to the absorber. It can be seen that when the bulk composition of the reactor is around stochiometric conditions, it is far from the equilibrium composition. In fact, around stochiometric compositions, $c_{CO_2(aq)}$ is close to zero, and the

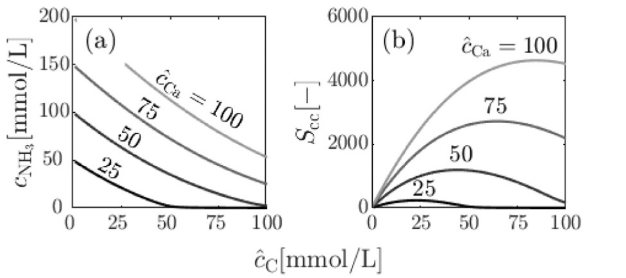

Fig. 3. (a) concentration of ammonia, $\hat{c}_{NH_3}$, as a function of $\hat{c}_C$ and $\hat{c}_{Ca}$, (b) the saturation of calcium carbonation, S_{CC}, as a function of $\hat{c}_C$ and $\hat{c}_{Ca}$, furthermore $\hat{c}_{AN} = 0.25$ M and $T = 25^{\circ}$C.

driving force for absorption is solely determined by p_{CO_2} via Henry's law.

The absorption kinetics is governed by the conversion of CO_2(aq) near the gas-liquid interface into other species, this mainly happens via the following reaction [33]:

$$CO_2(aq) + 2NH_3(aq) \leftrightarrow NH_2COO^- + NH_4^+ \tag{4}$$

As the ammonia concentration is key for the absorption rate, it is interesting to analyze its behavior as a function of $\hat{c}_C$ and $\hat{c}_{Ca}$. This is illustrated in Fig. 3(a), which shows that by increasing the calcium content, c_{NH_3} increases, thus enhancing the absorption rate.

Precipitation of calcium carbonate can be represented by the following reaction:

$$CO_3^{2-} + Ca^{2+} \leftrightarrow CaCO_3(s) \tag{5}$$

The driving force for this reaction is given by the saturation of $CaCO_3$, S_{CC}:

$$S_{CC} = \frac{a_{CO_3^{2-}}\, a_{Ca^{2+}}}{K(T)} \tag{6}$$

The blue solid line in Fig. 2 is where $S_{CC} = 1$, i.e., the thermodynamic equilibrium; the grey dotted arrow, labelled "precipitation", represents the change of composition due to the precipitation of $CaCO_3$, note that this lies on the diagonal due to the reaction stochiometry. Fig. 3(b) shows S_{CC} as a function of $\hat{c}_C$ and $\hat{c}_{Ca}$; it is worth noticing that the saturation is highest around stochiometric conditions. Hence, it is expected that the precipitation performance is best around stochiometric conditions between total calcium and total carbon in the solution.

Absorption and precipitation are represented in Fig. 2 by the arrows as two separate events, but in fact, they happen simultaneously in the absorber. Therefore, the steady state composition in the continuously operated absorber is a combination of the absorption vector, and of the precipitation vector, whereby the distance from equilibrium, depends on precipitation kinetics. In Fig. 2 the composition in the absorber is represented by the red cross. In the growth reactor only precipitation occurs, i.e., its composition is simply further down the precipitation vector towards the equilibrium, as represented depicted by the blue cross.

2.3. Precipitation in the dissolution reactor

Even in an ideal scenario where equilibrium is reached in the growth reactor, i.e., the composition is on the blue line of Fig. 2, the steady state of the solution after the growth reactor is not in the origin. Hence there is carbon and calcium in the solution that is fed back to the dissolution reactor. This carbon will precipitate after fresh calcium dissolves, as this increases the supersaturation of $CaCO_3$. There are two possibilities for the composition of the solution fed to the dissolution reactor: (i) there is more calcium than carbon dissolved, which will increase the final calcium concentration in the dissolution reactor, or (ii) there is more carbon than calcium dissolved, which will decrease the final calcium concentration in the dissolution reactor. Essentially this changes the effective amount of calcium fed to the dissolution reactor, which is referred to as $\hat{n}_{ca,corr}$, and may be estimated as:

$$\hat{n}_{Ca,corr} = \hat{n}_{Ca,0} - L/S\,(\hat{c}_{C,G} - \hat{c}_{Ca,G}) \tag{7}$$

Here $\hat{c}_{C,G}$ and $\hat{c}_{Ca,G}$ are the carbon and calcium concentration in the growth reactor, respectively. Operating at non-stochiometric conditions may be either due to a lack of control as it is difficult to know the liquid concentrations during operation, or it is done onpurpose to achieve a specific goal (see Section 4.3.3).

The $CaCO_3$ formed in the dissolution reactor will leave the plant as part of the leached RCA, and is not part of the PCC product stream (see Fig. 1). Thus, two production rates should be accounted for, one for the amount of PCC produced in pure form in the carbonation section, and one for the total amount of CO_2 converted to $CaCO_3$ (see Section 3.3.3).

2.4. Changes in mother liquor

Introduction of impurities or evaporation of ammonia may change the thermodynamics of the system, i.e., the solution may become more acidic or alkaline. This shifts the equilibrium compositions for dissolution, absorption and precipitation in the $\hat{c}_{Ca}$, $\hat{c}_C$ diagram, up or down respectively. This is illustrated in Fig. 4 for a 0.25 M AN solution: (a) by the dash-dot line for a solution depleted in ammonia (10 %), and (b) for the introduction of 10 mmol of strong acidic or alkaline species. Therefore, the steady state calcium concentrations may increase or decrease when the solution becomes more acidic or more alkaline.

3. Equipment and method

First in Section 3.1, the design of the plant and the rationale behind the equipment choice is outlined, as well as an overview of the materials used in the experiments. Section 3.2 summarizes the main practical issues which arised during the commissioning of the pilot unit. Then in Section 3.3: (i) the operational procedure for the pilot unit is described, (ii) the samples and measurements taken during the experiments are presented, and (iii) the processing of the measured data into relevant parameters is reported. Finally, in Section 3.4, the experimental procedure for the material tests with the products obtained from the pilot plant is described.

3.1. Pilot plant equipment

3.1.1. Plant design

The plant had to fulfill a set of key specification, namely:

- The plant had to be mobile in order to allow for the planned tests at the two different locations, and potentially at other locations in the future.

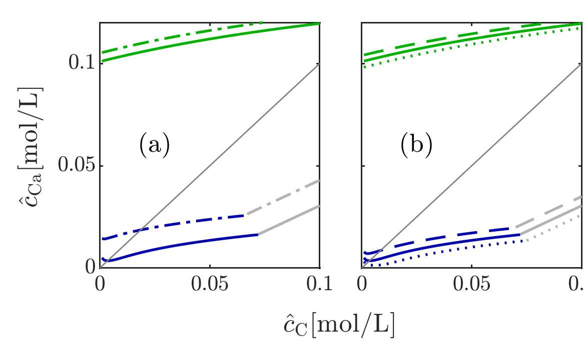

Fig. 4. The effect on the thermodynamics of a 0.25 AN solution, (a) after 10 % evaporation of NH_3 (dot-dash), and (b) addition of 10 mM acidifying (dashed) or alkaline species (dotted).

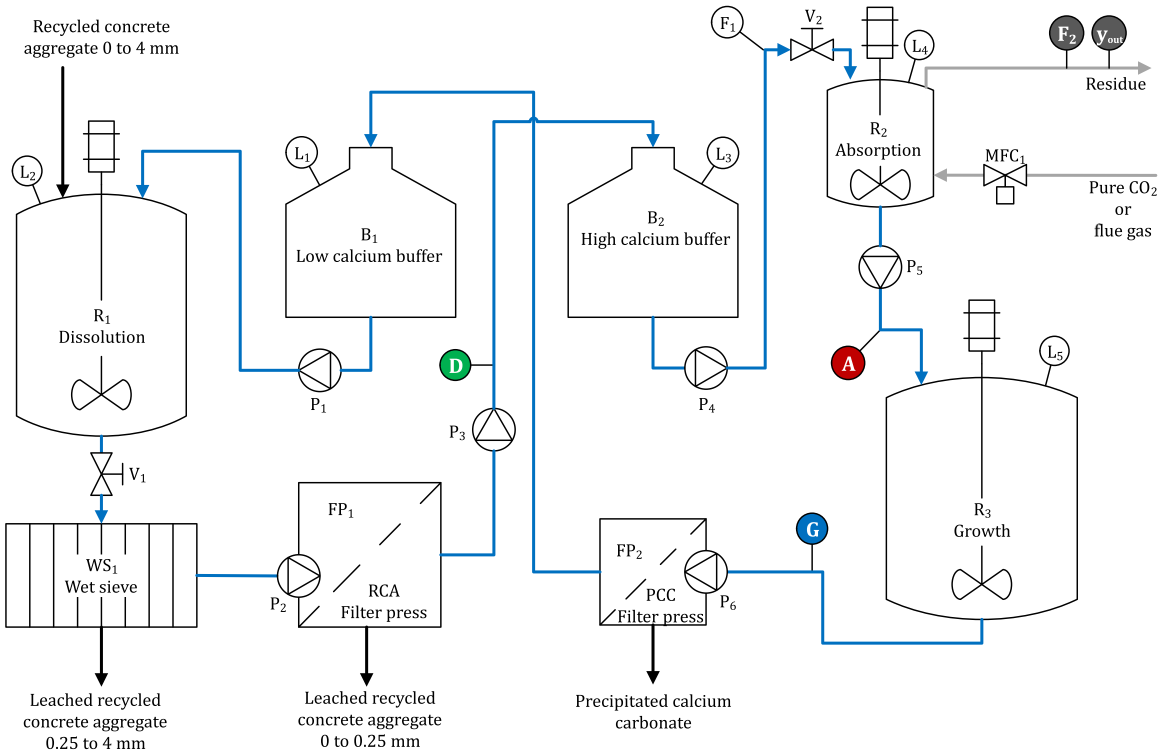

Fig. 5. Simplified P&ID of the pilot plant showing the main components, instruments, and sampling points.

Fig. 6. The container containing the dissolution side of the process with from right to left: the calcium rich buffer, the dissolution reactor, the wet sieve, and the RCA fines filter press.

- The production capacity had to be such that it enabled material tests with both the leached fines and the precipitated calcium carbonate, i.e., the production rates of both products had to be at kilogram scale.
- The plant had to be able to operate at a variety of operating conditions, allowing variations of: the liquid flowrate, Q, the solid loading, S/L, the ammonium nitrate concentration, $\widehat{c}_{AN}$ and the CO_2 inlet flow rate, $F_{CO2,in}$.
- The equipment to carry out the different steps had to be be industrially relevant and scale, i.e., no laboratory scale.
- The plant had to be operable by a maximum of two persons, preferably by one person only.

A simplified P&ID of the plant is shown in Fig. 5, photographs of the two containers in which the equipment is mounted are shown in Figs. 6 and 7, and a detailed component list can be found in the appendix. Based on the above list, a plant capable of handling up to 160 kg fines per hour (corresponding to producing a few kg of PCC per hour), with a S/L up to 0.4 was selected. Consequently the liquid flow through the plant was designed for up to 400 L/h, while being adjustable. The residence time in the batch dissolution reactor (R_1) was chosen to be $t_D = 30$ min (including emptying), i.e., limited to the first, most effective part of the dissolution process [25], resulting in a reactor volume for R_1 of 200 Liters. The volumes for the absorption reactor (R_2) and the growth reactor (R_3) were decided to be 100 and 200 liters respectively, resulting in volume ratios that are expected to work well based on laboratory tests. Buffers (B_1 and B_2) with a volume of 1000 liters are placed between the dissolution and the carbonation side of the process to accompany the batch operation of the former and continuous operation of the latter; during operation these buffers are only partially filled, however, large buffers enable easy startup (see Section 3.3.1). All vessels

Fig. 7. The container containing the carbonation side of the process from left to right: the absorber, the growth reactor, the calcium carbonate filter press and the calcium-lean buffer.

are equipped with continuous level sensors (L_1 to L_5) for process control. The reactors are equipped with agitators (M_1 to M_3) for proper mixing.

The pumps P_1 to P_3, operating in batch mode to fill or to empty the dissolution reactor, are high capacity pumps chosen as to keep the cycle time of the dissolution step as desired; P_1 and P_3 are centrifugal pumps and P_2 is a pneumatically driven piston pump. Pumps P_4 to P_6 are operating in a continuous mode; centrifugal pumps P_4 and P_5 are controlled via frequency regulators, and piston pump P_6 operates in a short cyclic on/off mode (see Section 3.3.1).

The feed gas, available at 6 bar, is fed to the absorption reactor at ambient pressure via a mass flow controller (MFC_1). The gas is dispersed in the bottom of the absorption reactor via two sinter metal spargers (2×30 cm^2, 5 μm pores).

For the solid-liquid separation after the dissolution stage, a two step approach was chosen to limit the size of the filter press, as this is a costly component: first, the larger particles ($\geq 250 \mu m$) are separated using a gravity fed vibrating wet sieve (WS_1), and then the smaller particles are separated using a filter press (FP_1) with a capacity of 15 L. For the PCC separation also a filter press was utilized (FP_2), with a capacity of 9 liter.

All equipment was placed in two 20 ft shipping containers connectable with flexible piping and electrical lines, thus resulting in an easily movable and installable plant. The plant was assembled by the manufacturing company Flexmet, and the electrical cabinets including control software was designed and built by NUKK engineering. The mode of operation, including the measurement protocol, is further discussed in Section 3.3.

3.1.2. Materials

While operating at the concrete site with pure CO_2 the RCA available on site and provided by Alluvia AG was used (RCA I, 0–4 mm, $\widehat{n}_{Ca,0} = 0.8$ mol/kg). For the experiments operated with flue gas at the Jura cement site, the fines were provided by Jura materials AG, sourced from one of their concrete sites (RCA II, 0–4 mm, $\widehat{n}_{Ca,0} = 1$ mol/kg). Pure CO_2 was delivered in a bundle of twelve 50 liter tanks (Carbagas, 99.99 % pure), with a pressure regulator set at a pressure of 6 bar. The flue gas (between 16 and 20 vol %, CO_2 content) was taken from the stack at the Jura cement plant in Wildegg by means of a compressor via a cooler, delivering the gas to the mass flow controller (MFC_1) at the required pressure of 6 bar and at the operating temperature. To prepare the solvent, a concentrated ammonium nitrate solution of 6.43 mol/kg (fertigro AN, 25 kg cannisters) was diluted with tap water in buffer tank B_1.

3.2. Practical considerations

During commissioning of the pilot unit several practical issues surfaced that are worth reporting here. The main issues, possible solutions, and remaining challenges are grouped in four categories: (i) corrosion, (ii) solvent residue conductivity, (iii) fouling, and (iv) difficulties during dissolution.

3.2.1. Corrosive nature of solvent and flue gas

Aqueous ammonium nitrate is weakly acidic and therefore corrosive in nature. In principle the plant was designed such that all equipment in contact with the solution was made of materials able to withstand such a solution. However, in reality, spillage occurs, as well as evaporation of ammonia, which is corrosive too; this degrades components which are in principle not in contact with the solution. In general one should take care that components are physically separated from both the solution and its vapor, or one should make sure that components are made of materials that can withstand these corrosive environments.

3.2.2. Conductive nature of the solvent residue

The plant had several level switches installed to prevent overflow of vessels (these are not used during operation and are merely a safety feature); these operate by detecting a conductive path, i.e., a conductive liquid, between two electrodes. The issue with aqueous ammonium nitrate is that the residue left after submersion was conductive as well, i.e., the sensors do not always turn off after they turned on. Therefore, level sensors based on conductivity will not function properly and alternative solutions have to be used, e.g., sensors based either on displacement or on optics.

3.2.3. Fouling in the carbonation side

Fouling in crystallization processes is a common problem, and this is no exception. In the carbonation side of the process fouling occurs, mostly in the absorption vessel (R_2) and in the following pump (P_5), where supersaturation is highest. The fouling process is slow and is manageable by regular maintenance using acidic cleaning agents.

3.2.4. Dissolution side operation

The dissolution side of the process was difficult to operate as it required that the dissolution reactor outflow (R_1), the throughput of the wet sieve (WS_1), and the throughput of the filter press (FP_1) are similar. However, the outflow of R_1 during emptying is much higher in the beginning than at the end, requiring flow control (in the plant this is done manually). At the same time, the filter press throughput decreases as it fills up with solids, requiring emptying every 2–3 cycles, and as a consequence not exploiting the total capacity of the filter press. With proper automation, these difficulties may be resolved; however, it is likely that other concepts are better suitable from an operational perspective, e.g., dissolution taking place in a bed packed with the particles of RCA.

3.3. Experimental methodology

3.3.1. Operation of the pilot plant

Before starting, the calcium-lean buffer is filled with 1000 liters of aqueous ammonium nitrate solution at the desired concentration $\widehat{c}_{\mathrm{AN}}$. Then, the process is initiated, consisting of the following steps:

- The dissolution reactor is filled with the ammonium nitrate solution; when filled, the appropriate amount of RCA is dosed and a timer starts.
- When the timer reaches the set-point τ_{set}, the vibrating wet sieve starts, the outlet valve V_1 is opened, and the inlet and outlet pumps of filter press 1 start.
- The solids are collected at the outlet of the wet sieve ($\geq 250\ \mu m$) and inside filter press 1 ($< 250\ \mu m$), while a clear solution with high calcium content is collected in the calcium-rich buffer.
- When the dissolution reactor is empty (emptying takes ca. 5 min), the valve is closed, the solid-liquid separation stops, and the dissolution reactor is filled again with the solution from the calcium-lean buffer.

This cycle, the dissolution cycle, taking $\tau_D \approx \tau_{\mathrm{set}} + 5$ min, is repeated during the experiment. After 2 dissolution cycles, when approximately 400 liters of a clear calcium-rich solution is in the calcium rich buffer, the carbonation part of the plant starts:

- The absorber feed pump starts and the liquid inlet valve (V_2) is regulated by hand such that it the flow, Q, is at the set-point on the flow meter (F_1).
- At the same time when the absorber feed pump starts, the gas flow starts and MFC_1 controls the gas flow as required.
- As soon as the absorber is filled, the growth reactor feed pump starts and a PID controller adjusts the growth reactor feed pump to keep the level in the absorber as desired.
- Once the growth reactor is filled, the pump of filter press 2 turns on for 30 s, pumping the suspension containing PCC through the filter press, and decreasing the level in the growth reactor somewhat below the set-point; thereafter this repeats continuously.
- The PCC is separated and stays in the filter press, while the clear calcium-lean solution is transferred into buffer 1.

Filter press 1 is opened and emptied every 2–4 cycles, depending on the value of S/L; filter press 2 is only emptied at the end of an experiment, i.e., not during operation.

3.3.2. Measurements

A minimum of 6 dissolution cycles are performed in each experiment to reach steady state, when samples are withdrawn, namely liquid samples from the points D, A, and G, and solid samples are taken from A and G (see Fig. 5). The liquid samples are analyzed using ion chromatography (IC), resulting in concentration measurements $\widehat{c}_{i,\mathrm{D}}$, $\widehat{c}_{i,\mathrm{A}}$ and $\widehat{c}_{i,\mathrm{G}}$ respectively. The solid samples are analyzed using X-ray diffraction (XRD) to determine morphology and/or with laser diffraction to obtain the particle size distributions (PSD). For pure CO_2 feed, the gas outflow is measured with flow meter F_2, and for flue gas feed the CO_2 concentration, y_{out}, is measured with a gas analyser. The latter may be converted into CO_2 flow rate, $F_{\mathrm{CO_2,out}}$, using the following equation, that is obtained through the material balance of nitrogen, which is assumed to remain in the gas phase:

$$F_{\mathrm{CO_2,out}} = \frac{y_{\mathrm{out}}(1-y_{\mathrm{in}})F_{\mathrm{in}}}{1-y_{\mathrm{out}}} \tag{8}$$

Here F is a flow rate in mole per hour and y is a mole fraction. In the results section the calcium concentration measurements are reported as is, the CO_2 flows are converted to make them easily comparable to the calcium concentrations:

$$f_{\mathrm{CO_2,feed}} = F_{\mathrm{CO_2,in}}/Q \tag{9a}$$

$$f_{\mathrm{CO_2,absorbed}} = (F_{\mathrm{CO_2,in}} - F_{\mathrm{CO_2,out}})/Q \tag{9b}$$

here Q denotes the liquid flow rate in the plant. Furthermore it is convenient to define the ratio of carbon and calcium in the solution:

$$\psi = \frac{f_{\mathrm{CO_2,absorbed}}}{\widehat{c}_{\mathrm{Ca,D}}} \tag{10}$$

3.3.3. Performance indicators

In order to assess and to compare the steady state performance of the plant at different operating conditions, it is useful to translate the physical measurements into a set of performance metrics:

1. The CO_2 storage rate, $s_{\mathrm{CO_2}}$, which is defined as the moles of CO_2 fixed as $CaCO_3$ per unit time. This includes the precipitation in the dissolution reactor, i.e., it is equivalent to all the CO_2 that is absorbed in the whole plant:

$$s_{\mathrm{CO_2}} = F_{\mathrm{CO_2,in}} - F_{\mathrm{CO_2,out}} \tag{11a}$$

2. The PCC productivity, p_{cc}, which is defined as the amount of PCC produced in moles per hour in the carbonation section, and exits the plant as pure PCC; it excludes the precipitation occurring in the dissolution reactor:

$$p_{\mathrm{cc}} = Q \quad \left(\widehat{c}_{\mathrm{Ca,D}} - \widehat{c}_{\mathrm{Ca,G}}\right) \tag{11b}$$

3. The calcium efficiency, η_{Ca}, being the fraction of precipitated calcium with respect to the available dissolvable calcium in the feedstock to the plant:

$$\eta_{\mathrm{Ca}} = \frac{s_{\mathrm{CO_2}}}{(S/L)\ Q\ \widehat{n}_{\mathrm{Ca,0}}} \tag{11c}$$

4. The carbon efficiency, η_{C}, being the fraction of precipitated carbon with respect to the carbon fed to the plant:

$$\eta_{\mathrm{C}} = \frac{s_{\mathrm{CO_2}}}{F_{\mathrm{CO_2,in}}} \tag{11d}$$

5. The solvent utilization, u_{AN}, which is the ratio of the total amount of CO_2 precipitated over the amount of ammonium nitrate that is lost:

$$u_{\mathrm{AN}} = \frac{s_{\mathrm{CO_2}}}{W\ (S/L)\ Q\ \widehat{c}_{\mathrm{AN}}} \tag{11e}$$

Here W is the solvent retention in the solids after filtration (without washing steps), in mass of solvent per unit mass of solids, which was measured in our experiments to be about $W = 0.15$.

Table 2
Overview of the mortar mixes (by weight) used in the compressive strength tests.

	tests 1		tests 2		
CEM I	22.2 %	22.2 %	16.7 %	16.7 %	16.7 %
Limestone			**5.5 %**		
PCC as produced				**5.5 %**	
PCC ground					**5.5 %**
Water	11.1 %	11.1 %	11.1 %	11.1 %	11.1 %
Sand			66.7 %	66.7 %	66.7 %
Fresh RCA	**66.7 %**				
Leached RCA		**66.7 %**			

Note that η_{Ca}, η_C, and u_{AN}, may be defined with either the storage rate, s_{CO_2}, or the PCC production rate, p_{cc}, as reference. Here the storage rate, s_{CO_2}, is used as reference, as the fundamental purpose of this technology is fixing carbon for the purpose of climate mitigation.

3.4. Material tests

The goals of the material tests are the following:

I. To evaluate the performance of the leached RCA in comparison to the fresh RCA as aggregate in concrete.
II. To evaluate the possibility of using the PCC as a replacement for ground limestone in the widely used cement, grade CEM II.

Fresh and leached RCA are compared by evaluating the compressive strength development of mortars made using the two types of RCA as sand component. The PSDs of fresh and leached RCA were reconstructed in order to avoid differences between them; the reconstructed PSD can be found in the appendix. As RCA is known to have high water absorption, the water absorption of both fresh and leached RCA was determined according to a standardized protocol from an internationally recognized norm (SN EN 1097–6). Extra water was added to the mortar mixes to compensate for the water absorbed, as to achieve equal amounts of available water for the curing process.

To assess the possibility of using the PCC as main constituent for cement production, PCC and ground limestone were mixed with CEM I, and the compressive strength of mortars were evaluated. One fraction of the PCC was used with the particle sizes as it was produced ($\sim 30\mu$m), and the other fraction was ground to obtain finer particles ($\sim 2\mu$m), similar in size to those in the limestone (see appendix for PSDs).

The mortar prisms ($40 \times 40 \times 160$ mm^3) subject to the tests were produced based on an established norm (SN EN 196–1), which defines a mortar mix recipe and a test protocol. In tests I, the sand fraction was replaced by either RCA or leached RCA, and in tests II, a quarter of the cement was replaced with ground limestone, PCC as produced, or ground PCC. The (not absorbed) water to cement ratio was 1:2, while the sand to cement ratio was 3:1; an overview of all mortar mixes is provided in Table 2. The compressive strengths of mortar prisms were tested after 2 days, 7 days, and 28 days of curing; the results are presented and discussed in section 4.4.

4. Experimental results

First, in Section 4.1, the reproducibility and stability of the operational procedures are assessed. After that, the changes of the mother liquor composition over many dissolution cycles and the related effects are discussed in Section 4.2. Then in Section 4.3, the steady state results for both types of feed, i.e., pure CO_2 and flue gas, are reported, followed by their analysis in terms of performance parameters, defined by Eqs. (11a) to (11e); an overview of the experiments performed and their operating conditions is provided in Table 3. Finally, the material test results obtained with the products from the process, i.e., leached RCA and PCC, are reported and discussed in Section 4.4.

4.1. Reproducibility and stability

At the start of the experimental campaign, three experimental runs under the same operating conditions and the same mother liquor were performed on three consecutive days (exp 1a, 1b, 1c). Then later in the campaign the experiment was repeated once more, about 50 dissolution cycles later, again with the same mother liquor (exp 1d). The experiments were performed with pure CO_2 at liquid flow rate, $Q = 400$ L/h, solid loading $S/L = 0.2$, ammonium nitrate concentration $\widehat{c}_{AN} = 0.25$ M, and CO_2 inlet flow rate, $F_{CO2,in} = 0.8$ kg/hr; the choice was made targeting a stochiometric ratio of carbon and calcium in the carbonation section, i.e., to have $\psi = 1$.

Fig. 8 shows the measurements of experiments 1 and also those of experiment 2, that are already considered here for comparison (a detailed comparative discussion of this and other experiments follows in 4.3). These are the key observations from Fig. 8: (i) The liquid concentration measurements are quite stable, the coefficient of variation for the liquid phase measurements, averaged over the four experiments, is $CV_c = 8$ %. (ii) The calcium concentration levels increase slowly from experiment 1a to experiment 1d due to changes in the mother liquor, as discussed separately in Section 4.2. (iii) There is no gas outflow from experiments 1, i.e., all CO_2 is absorbed, the coefficient of variation of the relative flows, f, is therefore estimated using experiment 2 at steady state, resulting in $CV_{f,\mathrm{pure}} = 5\%$. Furthermore, in the experiments with flue gas, the feed CO_2 molar fraction, $y_{CO2,in}$, varied between 15 mol % and 20 mol %, thus leading to a major uncertainty when using Eqs. (9a) and (9b). Therefore, in the calculations, an average of 17.5 mol % with a standard deviation of 2.5 mol % is assumed for $y_{CO2,in}$. From this the coefficient of variation of the relative flows, f, for flue gas was estimated at $CV_{f,\mathrm{flue}} = 15$ %. This is rather high but intrinsic to the cement plant flue gas, and limits the analysis that can be done with the results of the experiments with flue gas (see Section 4.3.2).

Table 3
Overview of the experiments performed with the pilot unit and of their operating conditions; experiments are listed in chronological order: experiments 1a, 1b, 1c and 1d are repetitions at the same operating conditions.

Nr	Feed gas	Solids feed	F_{in} [kg/h]	S/L [–]	Q [L/h]	$\widehat{c}_{AN}$ [M]	T [∘C]
1a	pure CO_2	RCA I	0,8	0,2	400	0.25	15
1b			0.8	0.2	400		
1c			0.8	0.2	400		
2			**1.2**	0,2	400		
3			**1.2**	**0.4**	400		
1d			0.8	0.2	400		
4			**0.6**	0.2	**200**		
A	flue gas	RCA II	6	0.2	400	0.25	15
B			6			**0.4**	15
C			**4.5**			0.25	**5**

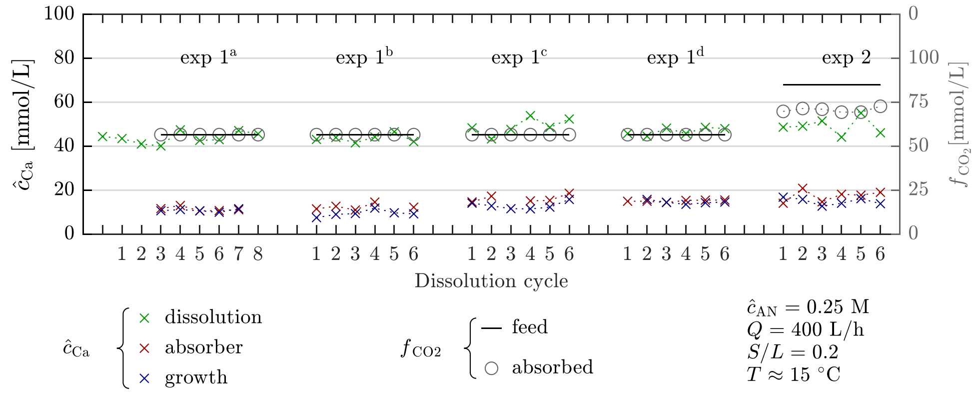

Fig. 8. The results of the four reproducibility experiments (exp 1a, 1b, 1c, 1d), and those of an experiment with increased gas feed flow (exp 2).

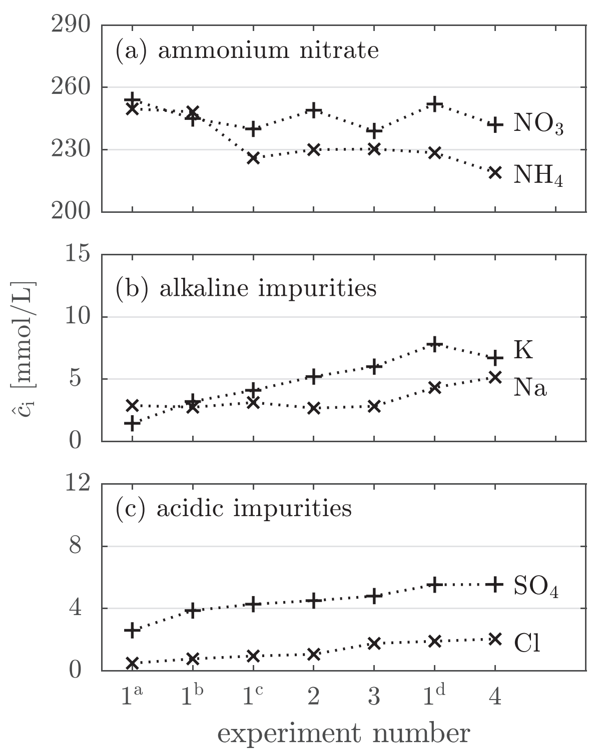

Fig. 9. (a) Ammonium nitrate progressions and (b), (c), impurities build-up in the mother liquor over eight experiments, corresponding to roughly 80 dissolution cycles.

4.2. Changes in mother liquor composition

Fig. 9 shows the apparent steady state concentrations of the constituent species of the catalyst, NO_3 and NH_4, and of the main impurities, K, Na, SO_4 and Cl, for the experiments with pure CO_2 (~ 80 dissolution cycles in total). Traces of other species were also measured, however they were stable at insignificant amounts and are therefore not reported here for the sake of clarity. Note that the data are plotted in chronological order, from the first to the last experiment.

Fig. 9(a) shows that there is a decrease in ammonia content, especially during the first three experiments. This is due to evaporation in the dissolution section: when the solution is high in calcium the speciation is high in NH_3(aq), which evaporates while the solution is exposed to the environment during wet sieving. This effect is confirmed by a light ammonia smell present during the wet sieving and is also known from literature [19,34].

Fig. 9(b) and (c) show the evolution of the main alkaline and acidic impurities, respectively, which dissolve into the mother liquor from the RCA; it can be seen that K, Na, SO_4 and Cl increase over time and seem to reach a plateau. Nevertheless, realizing that SO_4 is associated with a diacid, one can see that the acidic and alkaline compounds roughly cancel, therefore the effects on the thermodynamics are negligible (see Fig. 4 (b)). Therefore, the changes in the behavior of the mother liquor is dominantly due to the evaporation of ammonia, i.e., the mother liquor acidifies, and the calcium concentrations throughout the plant increases slightly and then stabilizes. This behavior is confirmed by experiments 1a to 1d (see Fig. 8), and the results show that solvent may be recycled about 50 times without significant changes, which is in line with the replacement rate of the process.

4.3. Steady state results and performance

4.3.1. Results for 100 % CO_2

Fig. 10 shows the steady state results of the experiments with pure CO_2 feed. The effects of the following parameters are investigated: $F_{CO_2,in}, S/L$ and Q, whose specific values are reported in the top of the figure.

The experiments demonstrate that the plant works properly at a variety of operating conditions, and is able to store CO_2 sourced from a pure feed in the form of $CaCO_3$, thus confirming the technical feasibility of the process with industrially relevant equipment. For the tested conditions, the growth reactor does not increase the precipitation significantly, as the absorber compositions are already close to equilibrium. Furthermore, in all experiments dissolved CO_2 is fed back to the dissolution reactor (as indicated by the hatching in the grey bar), causing precipitation there. Comparing experiment 1^c and 2 shows that the increase in gas flow beyond stochiometric conditions has a negative effect on the precipitation rate, as predicted according to the thermodynamic framework (see Section 2). The excess of CO_2 fed back to the dissolution reactor results in a slightly lower calcium concentration there (see equation (7)). Besides that, a large amount of the CO_2 fed is not absorbed and is thus lost. In exp 3, with $S/L = 0.4$, increased relative to experiment 2, the calcium concentration in the dissolution reactor is enhanced, which improves the absorption (see Fig. 3(a)); the combination of high reactant concentration and ψ close to 1, resulted in a high precipitation rate. Exp 4, with $Q = 200$ L/h and $F_{in} = 0.6$ kg/h, corresponds to experiment 2, but with the residence times doubled. However, the relative amount of absorbed CO_2 is higher for experiment 4, leading to $\psi \gg 1$, i.e., slow precipitation and a high excess of CO_2 fed back to the dissolution reactor. Consequently, a decrease in calcium concentration in the dissolution reactor was observed (see equation (7)), opposite to what one would expect from an increase in residence time.

4.3.2. Results with flue gas

Fig. 11 shows the steady state results for 3 sets of different operating conditions using flue gas, varying $\hat{c}_{AN}$ and T; the specific values of the

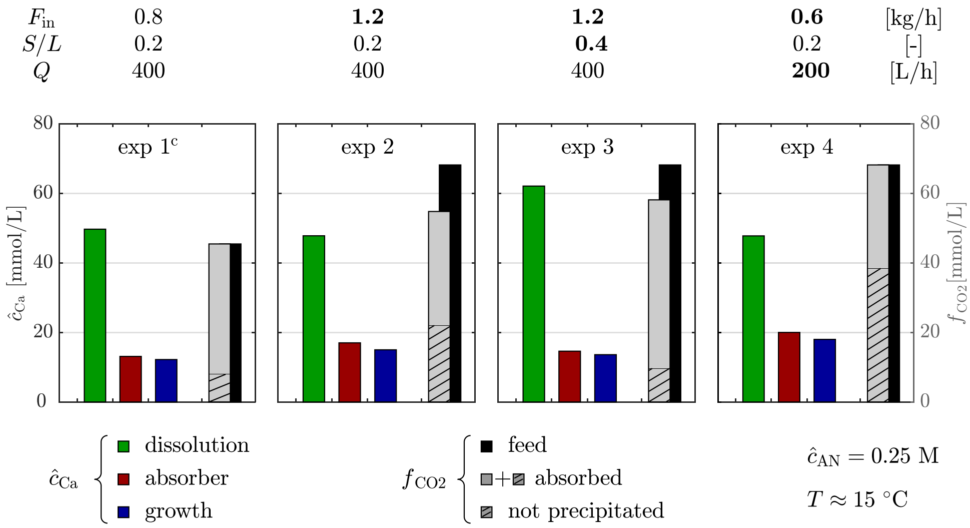

Fig. 10. Steady state results of the experiments performed with pure CO_2.

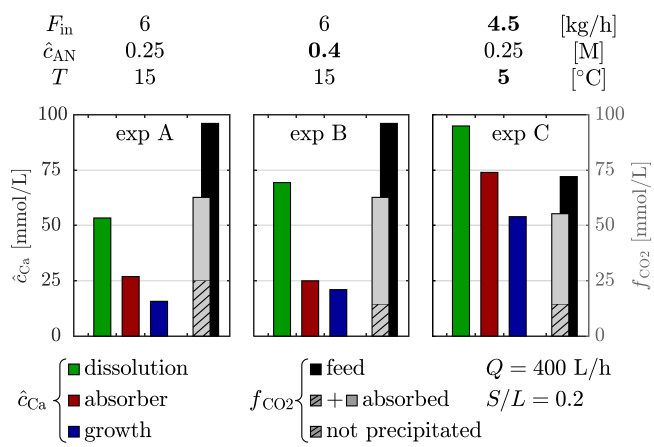

Fig. 11. Steady state results of the experiments performed with flue gas.

operating conditions are reported at the top of the figure.

The experiments demonstrate that the plant is able to store CO_2 as $CaCO_3$, confirming the technical feasibility with using industrial flue gas as feed at pilot scale. Due to the high uncertainty of the CO_2 content in the feed (see Section 4.1), it is hard to analyze the results in detail. Nevertheless the following observations can be made: All experiments exhibit significant CO_2 losses; the lower CO_2 partial pressure of flue gas requires higher feed flows to get to $\psi = 1$. Also, the experiments exhibit higher calcium concentrations in the dissolution step than when using pure CO_2 at comparable conditions. This is related to the higher calcium content in the RCA used. Comparing exp A and exp B suggests that a higher ammonium nitrate concentration increases the calcium concentration in the dissolution step, as it increases the solubility. The increase in calcium resulted in a stochiometric ratio ψ closer to 1, which improved the precipitation rate. Finally, exp C at $T = 5$°C had so low precipitation rate, that calcium builds up in the system. This build-up enhances the precipitation rate until a steady state between dissolution, absorption, and precipitation is established at higher calcium concentrations. Worth noting is that under these circumstances the growth reactor is a very useful addition, and that the precipitation rate is not lower than that in exp A.

4.3.3. Performance of the pilot unit

The steady state may be characterized in terms of the five performance parameters, $s_{CO_2}, p_{CaCO3}, \eta_C, \eta_{Ca}$ and u_{AN} (see Section 3.3.3);

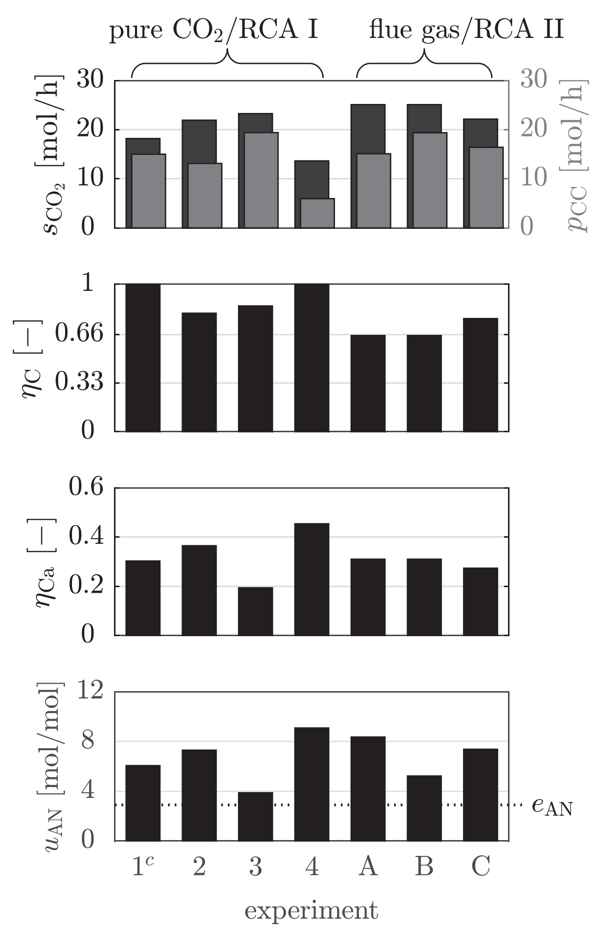

Fig. 12. steady state behavior of the pilot plant in terms of the performance parameters, $s_{CO_2}, p_{CC}, \eta_C, \eta_{Ca}$ and u_{AN}.

Fig. 12 shows these performance parameters for all the steady state results presented in this section. For reference, in the solvent utilization plot, the specific CO_2 emissions for ammonium nitrate production, $e_{AN} = 2.9 \mathrm{mol}_{CO_2}/\mathrm{mol}_{AN}$, is indicated with the dotted line [35,36].

The main points from the figure are as follows:

1. The carbon efficiencies for pure CO_2 are better than those for flue gas as the partial pressure of the former induces a higher driving force for absorption than the latter.
2. Feeding RCA with high calcium content increases the production rates, as it is visible from similar experiments with RCA I/pure CO_2 versus those with RCA II/flue gas.
3. An excessive amount of CO_2 absorbed, i.e., $\psi \gg 1$, leads to large differences between s_{CO_2} and p_{CaCO3}, as can be seen in experiments 2, 4 and A.
4. The production rate is increased by a higher value of S/L (see exp 3); the trade-off is lower solvent utilization as the relative increase in wet solid outflow is higher than the performance increase.
5. An increase in $\widehat{c}_{AN}$ enhances the production rate (see exp B); as the performance enhancement is not proportional to the increase in $\widehat{c}_{AN}$, the ammonium nitrate utilization is reduced.
6. All calcium efficiencies are rather low, this comes from the intrinsic nature of calcium dissolution from RCA in a batch reactor [25,28].
7. As there is no washing step, the AN usage is in the same order of magnitude as the emissions from AN production, hence a washing step is required for IMC to be ecologically viable.

Points 1 and 2 are fixed by operational circumstances, i.e, the feed stocks available, and point 3–5 relate to process optimization, e.g., maximizing the PCC production by setting $\psi = 1$. However, point 6 raises the question whether this dissolution concept is really the right one for this process/material combination, especially considering that the calcium efficiencies achieved in the simpler, direct mineral carbonation process are similar to what is achieved here [20]. Also, with reference to point 7, implementing the required washing in the current 2-step solid-liquid separation is tedious and would be expensive, and is not required for the direct process. Potentially different reactor concepts, e.g., a solid bed type system, can improve the calcium efficiency while at the same time simplifying implementation of a washing step [37].

4.4. Results of material tests

Material tests, as described in Section 3.4, were performed on the products of the process, i.e.: (I) fresh RCA versus leached RCA to evaluate its use as aggregate in concrete, and (II) PCC as produced and PCC ground versus ground limestone to evaluate its use as a filler in cement. The outcome of the tests are illustrated in Fig. 13; moreover, a summary of the properties of the materials used in the test is given in the appendix.

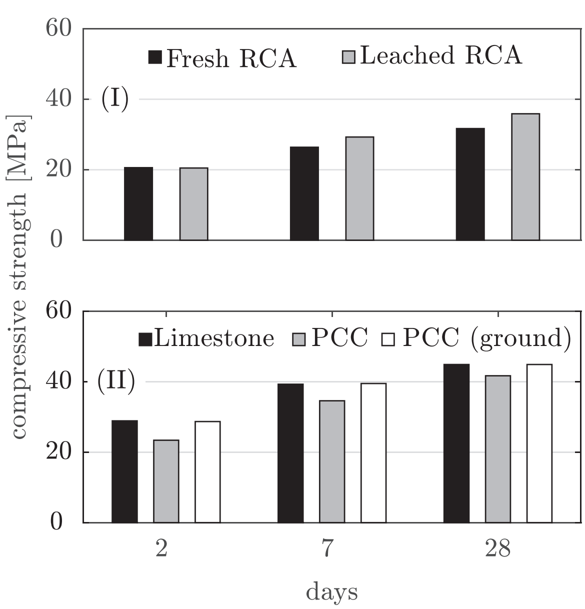

Fig. 13. Results of the material test comparing: (I) fresh RCA versus leached RCA, and (II) PCC as produced and PCC ground versus ground limestone.

Fig. 13 (I) compares the compressive strength of concrete using either fresh RCA or leached RCA as aggregates. The plot shows a minor increase in strength comparing leached RCA with fresh RCA after 7 days and 28 days, indicating that leached RCA is as good as, or even better than, fresh RCA for use as aggregate in concrete. An increase in concrete strength may reduce cement use, resulting in decreased emissions. These finding agree with previous research on directly carbonated RCA as aggregate in concrete, which suggests that carbonation yields an amorphous alumina-silica gel with pozzolanic properties [38], or it alters the so called inter-facial transition zone between the cement paste and the aggregate [39]. Globally, around 8 % of all aggregate used in concrete production is RCA [40,41], the rest being natural aggregates like sand. The results here indicate that this fraction of RCA may be replaced by leached RCA, with a potential improvement in concrete strength or a decrease in cement use.

Fig. 13 (II) compares the compressive strength of mortars using ground limestone, PCC as it is produced, or PCC ground, as a filler in cement. The results show that PCC as it is performs worse than ground limestone. However, when the PCC is ground to similar particle sizes as the limestone ($\sim 2\mu m$), the performance is similar, thus indicating that this material could be a suitable filler in cement. That being said, in industry, PCC can be used in higher value applications, and its use in concrete is likely not the most economically attractive one.

5. Conclusions

In this work, a mobile indirect mineral carbonation (IMC) pilot plant, capable of handling industrial flue gas as well as pure CO_2 as carbon feedstock, was constructed and operated thereafter, using 0–4 mm recycled concrete aggregate (RCA) as calcium feedstock.

After successful commissioning of the pilot unit, the experiments showed that the plant is able to store CO_2, sourced from either a pure feed or a flue gas, in the form of $CaCO_3$. Typically the plant processed around 80 kg/hr of RCA, while storing around 0.9 kg/hr of CO_2, corresponding to 2 kg/hr of $CaCO_3$. The results confirmed the technical feasibility and the stable operation of the process with industrially relevant equipment. Over the course of the experiments the composition of the mother liquor changed, mainly due to the light evaporation of ammonia, this acidifies the solution and increases the steady state calcium concentrations throughout the plant. However, the effects measured over roughly 50 dissolution cycles are small, which suggests a good recyclability of the ammonium nitrate solution. An important observation in the experiments is that, $CaCO_3$ precipitates after the carbonation section in the dissolution reactor, specifically when more than a stochiometric amount of CO_2 relative to dissolved calcium is absorbed. This decreases the PCC production rate, but not the storage rate as the $CaCO_3$ precipitated in the dissolution reactor simply leaves the plant as part of the leached RCA stream.

The plant may be operated at a variety of operating conditions and it responds to them as one would expect from thermodynamic considerations, e.g, increasing the solid loading or ammonium nitrate concentration increases the calcium concentration in the dissolution step. The trade-offs in terms of performance parameters are also as expected from thermodynamics and from laboratory scale tests, e.g., increasing the solid loading or ammonium nitrate concentration increases the production rates, but decreases the ammonium nitrate utilization. Another important observation is that the calcium extraction efficiencies are rather low, which is due to the thermodynamic nature of calcium dissolution from RCA in a batch reactor. Currently the plant has no washing step, hence the losses of ammonium nitrate are too high to be ecologically or economically feasible, as the emissions related to the ammonium nitrate losses are close to the amount of CO_2 stored. Potentially alternative reactor concepts for the dissolution side can improve the calcium extraction efficiency, the operational ease, as well as include a washing step, solving the main issues and limitations that were encountered.

The material tests suggested that leached RCA is as good, or even better, as fresh RCA for use as aggregate in concrete; the mechanisms behind this result are not fully understood and require more in-depth research. PCC as it is produced performs worse than ground up limestone as filler in cement, however, when the PCC is ground to similar particle size as the limestone the performance is identical. Although this indicates that it could potentially be used in cement, this is not the most economical one, as finely crushed PCC ($< 2\mu m$) may be used for higher value applications. Overall, the work has confirmed the technical feasibility and stable operation of IMC at scale in the concrete sector, while producing useful products. Although improvements are necessary to make the process economically and environmentally viable, i.e., better calcium extraction and solvent recovery, the work has been a steppingstone towards industrial implementation of IMC while generating operational experience at large scale.

CRediT authorship contribution statement

Mattheus Meijssen: Conceptualization, Methodology, Validation, Formal Analysis, Investigation, Data Curation, Writing - Original Draft, Visualization, Project administration. **Lena Marinello**: Methodology, Validation, Formal Analysis, Investigation. **Carmelo di Bella**: Methodology, Validation, Investigation, Writing - Review & Editing. **Antonio Gasós**: Writing - Review & Editing. **Marco Mazzotti**: Conceptualization, Writing - Review & Editing, Funding acquisition, Supervision.r.

Declaration of Competing Interest

The authors declare the following financial interests/personal relationships which may be considered as potential competing interests: Marco Mazzotti reports financial support was provided by Innosuisse Swiss Innovation Agency. Marco Mazzotti reports a relationship with Neustark AG that includes: consulting or advisory.

Data Availability

Data will be made available on request.

Acknowledgements

This research has received funding from the Swiss innovation agency Innosuisse (Grant ID 42739.1 IP-EE). The authors want to thank Marcel Eckstein, Luca Tschurtschenthaler and other employees of Neustark for the efforts they have put in the engineering and operation of the pilot unit. Also, we want to express gratitude to Jürg Hitz, Ken Wippich and other employees of Jura cement, as well as the employees of Alluvia, for helping with the installation and operation at their production sites.

Appendix A

A.1. Speciation model for the mother liquor

An aqueous solution with solutes consisting of the compounds, calcium, carbon, ammonia, nitrate, sodium and chlorine speciates into 18 different species as listed in Table 1.

When the apparent concentrations $\widehat{c}_{Ca}, \widehat{c}_{C}, \widehat{c}_{NH_4}, \widehat{c}_{NO_3}, \widehat{c}_{K}$ and $\widehat{c}_{Cl}$ are known, the concentration of the species in Table A1 can be determined. The following system of equations represent the chemical equilibrium reactions between the species in the solution:

$$a_{H_2O}/a_{H^+}a_{OH^-} = K_1 \quad (12a)$$

$$a_{CaOH^+}a_{H^+}/a_{H_2O}a_{Ca^{2+}} = K_2 \quad (12b)$$

$$a_{NH_3}a_{H^+}/a_{NH_4^+} = K_3; \quad (12c)$$

$$a_{HCO_3^-}/a_{CO_2(aq)}a_{OH^-} = K_4 \quad (12d)$$

$$a_{HCO_3^-}/a_{CO3_{2-}}a_{H^+} = K_5 \quad (12e)$$

$$a_{Ca^{2+}}a_{HCO_3^-}/a_{CaHCO_3^+} = K_6 \quad (12\ \ f)$$

$$a_{Ca^{2+}}a_{HCO_3^{2-}}/a_{CaCO_3(aq)}a_{H^+} = K_9 \quad (12\ \ g)$$

$$a_{Ca^{2+}}a_{NO_3^-}/a_{CaNO_3^+} = K_8 \quad (12\ \ h)$$

$$a_{NH_3(aq)}a_{HCO_3^-}/a_{H_2O}a_{NH_2COO^-} = K_9 \quad (12i)$$

$$a_{CaCl^+}/a_{Ca^{2+}}a_{Cl^-} = K_{10} \quad (12j)$$

$$a_{Na^+}a_{HCO_3^-}/a_{H^+}a_{NaCO3^-} = K_{11} \quad (12k)$$

A.1. The ions and molecules in the solution due to the speciation of calcium, carbon and ammonium nitrate in water

H^+	OH^-	Ca^{2+}	NH_4^+	$NH_3(aq)$	NO_3^-	$CaOH^+$	$CO_2(aq)$	HCO_3^-
CO_3^{2-}	$CaHCO_3^+$	$CaCO_3(aq)$	$CaNO_3^+$	NH_2COO^-	Cl^-	$CaCl^+$	Na^+	$NaCO_3^-$

Additionally, the overall mole balances for calcium, carbon, ammonia, nitrate, sodium and chlorine that have to be fulfilled, and are given by the following equations:

$$\widehat{c}_{\mathrm{Ca}} = c_{\mathrm{Ca^{2+}}} + c_{\mathrm{CaOH^+}} + c_{\mathrm{CaHCO_3^+}} + c_{\mathrm{CaCO_3(aq)}} + c_{\mathrm{CaNO_3^+}} + c_{\mathrm{CaCl^+}} \tag{13a}$$

$$\widehat{c}_{\mathrm{C}} = c_{\mathrm{CO_2(aq)}} + c_{\mathrm{HCO_3^-}} + c_{\mathrm{CO_3^{2-}}} + c_{\mathrm{CaHCO_3^-}} + c_{\mathrm{CaCO_3(aq)}} + c_{\mathrm{NH_2COO^-}} + c_{\mathrm{NaCO_3^-}} \tag{13b}$$

$$\widehat{c}_{\mathrm{NO_3}} = c_{\mathrm{NO_3^-}} + c_{\mathrm{CaNO_3^+}} \tag{13c}$$

$$\widehat{c}_{\mathrm{NH_3}} = c_{\mathrm{NH_4^+}} + c_{\mathrm{NH_3(aq)}} + c_{\mathrm{NH_2COO^-}} \tag{13d}$$

$$\widehat{c}_{\mathrm{Na}} = c_{\mathrm{Na^+}} + c_{\mathrm{NaCO_3^-}} \tag{13e}$$

$$\widehat{c}_{\mathrm{Cl}} = c_{\mathrm{CaCl^+}} + \widehat{c}_{\mathrm{Cl^-}} \tag{13 f}$$

Furthermore, as the overall solution is neutrally charged, an overall charge balance has to be fulfilled, i.e., the sum of a charges must be zero:

$$\sum(c_i z_i) = 0 \tag{14}$$

If the relations between activities and concentrations are known, this system of 18 equations (Equations (12a)a to (14)) has 18 unknowns (the concentrations of the species in Table A1) and can thus be solved. Concentration and activity are related to one another via the activity coefficients ($a_i = \zeta c_i$), these are calculated using the B-dot equation and is given by:

$$log(\zeta_i) = \frac{De_1 z_i^2 \sqrt{I}}{1 + d_i De_2 \sqrt{I}} + \dot{B}I \tag{15}$$

with I, the ionic strength given by:

$$I = \sum\left(0.5\left(c_i z_i^2\right)\right) \tag{16}$$

$De_1, De_2, \dot{B}$ and d_i are the Debye-Hunkel parameters, the B-dot parameter and the hard-core diameter for each species respectively. All these constants are coming come from a lookup table and have a dependency on temperature.

When all the concentrations and activities in the solution are calculated, the following relevant quantities may be calculated (see Theory section):

- The saturation of calcium hydroxide:

$$S_{CH} = \frac{a_{\mathrm{Ca^{2+}}} a_{\mathrm{OH^-}}^2}{K_{\mathrm{CH}}} \tag{17}$$

- The saturation of calcium carbonate:

$$S_{CC} = \frac{a_{\mathrm{CO_3^{2-}}} a_{\mathrm{Ca^{2+}}}}{K_{\mathrm{CC}}} \tag{18}$$

A.2. Component list of the pilot unit

Item	P&ID Code	Description
Containers	N/A	Owipex - Roll-off container 20"
Reactors	R_1	Polsinelli - 300 L boil pot
	R_2	B&R shop - Drucktank 2.5 B 120 Liter komplett
	R_3	B&R shop - Tank 250 Liter komplett
Level sensors	R_1, R_2, R_3	Kobold - Guided Radar Level Transmitter NGR-2242G5L
Stirrers	M_1, M_2, M_3	SRT-Mischer - SRT3–0–1500 High-speed mixer
Buffers	B_1, B_2	Auer packaging - IBC 1000 K 150.50-UN
Filter presses	FP_1	Simex - Mobile Filter Press SMM-2
	FP_1	Simex - Filterpress SLP 30 Modell 10/15
Wet sive	WS_1	Knauer engineering - Rüttelsieb VT10.5
Pumps	P_1, P_3	Ebara - centrifugal pump MATRIX 5–3 T/0,65

(continued on next page)

(*continued*)

Item	P&ID Code	Description
	P_4, P_5	Ebara - centrifugal pump JE 80 3 ∼ 230/400 V
	P_2, P_6	Simex - part of FP1 and FP2, Membrane pump TX70ANN
Flow meters and valves	MFC_1	Bronkchorst - Massflowcontroller F-203AV/F-213AV
	F_1	Kobold - MIM-1215HG5 C3T0
	F_2	SMC - Flowswitch PFM750s
	V_1	Nieruf - Ball valve
	V_2	Integrated in V2, ball valve
CO2 sensor	y_{out}	WITT - OxyBaby gasanalyzer

A.3. Properties of material used in RCA tests

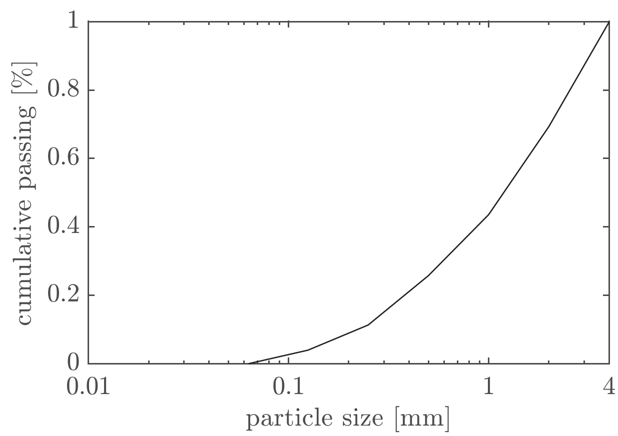

Fig. 14. The reconstructed PSD of the fresh and leached RCA leached used in the material tests.

.

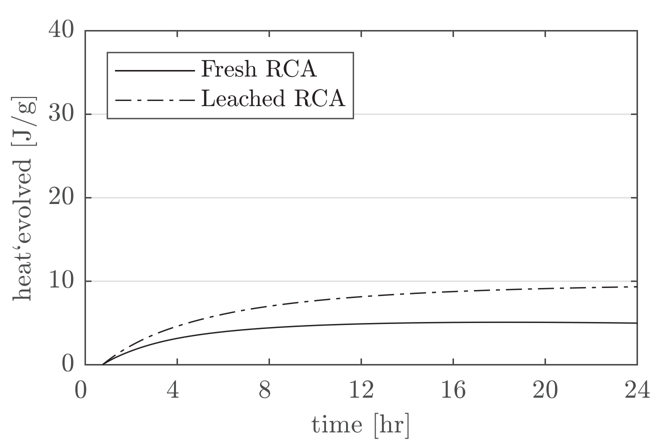

Fig. 15. Calorimetry of fresh RCA and leached RCA, for reference, cement hydration results in around 200 J/g after 14 h [42].

.

A.4. Properties of material used in PCC tests

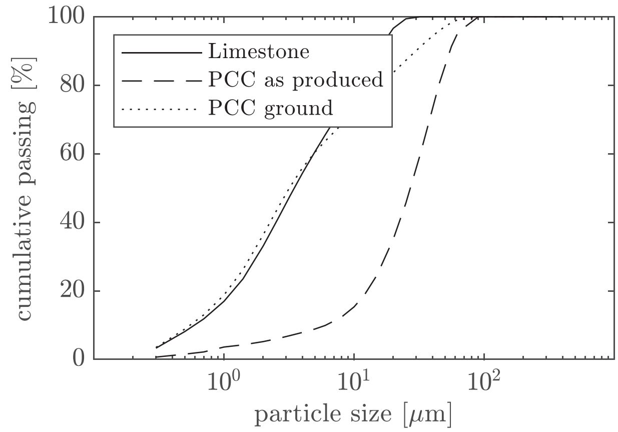

Fig. 16. The particle size distribution of the materials used in the material tests for PCC.

.

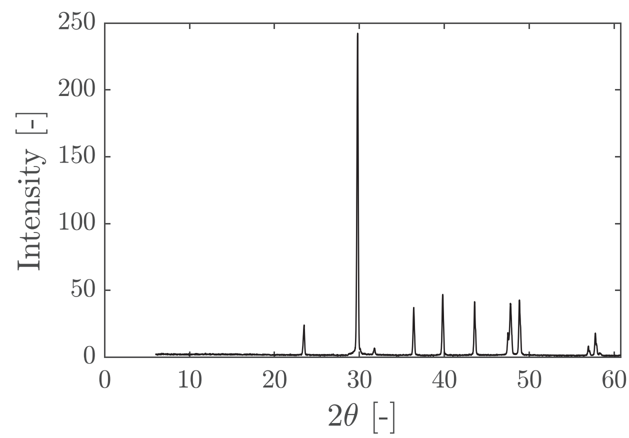

Fig. 17. XRD of the PCC that was used in the material tests, the pattern shows calcite.

.

References

[1] S.A. Miller, A. Horvath, P.J. Monteiro, Readily implementable techniques can cut annual CO_2 emissions from the production of concrete by over 20%, Environ. Res. Lett. (2016) 11.
[2] A. PetekGursel, E. Masanet, A. Horvath, A. Stadel, Life-cycle inventory analysis of concrete production: a critical review, Cem. Concr. Compos. 51 (2014) 38–48.
[3] G. Habert, S.A. Miller, V.M. John, J.L. Provis, A. Favier, A. Horvath, K.L. Scrivener, Environmental impacts and decarbonization strategies in the cement and concrete industries, Nat. Rev. Earth Environ. 1 (2020) 559–573.
[4] D.J.M. Flower, J.G. Sanjayan, Green house gas emissions due to concrete manufacture, Int. J. Life Cycle Assess. 12 (2007) 282–288.
[5] Habert, G. Environmental impact of Portland cement production, 2013, 3–25.
[6] D.N. Huntzinger, T.D. Eatmon, A life-cycle assessment of Portland cement manufacturing: comparing the traditional process with alternative technologies, J. Clean. Prod. 17 (2009) 668–675.
[7] Hasanbeigi, A., Price, L., Lin, E., Lawrence, E.O. A Review of Emerging Energy-efficiency and CO2 Emission-reduction Technologies for Cement and Concrete Production.2012.
[8] M. Voldsund, et al., Comparison of technologies for CO 2 capture from cement production—Part 1: Technical evaluation, Energies (2019) 12.
[9] J. Newman, B.S. Choo, Advanced concrete technology: concrete properties, Adv. Concr. Technol. (2003) 1–23.
[10] C.A. Horowitz, Paris agreement, Int. Leg. Mater. 55 (2016) 740–755.
[11] Sikora, A. European Green Deal - legal and financial challenges of the climate change.ERA Forum, 2020.
[12] J. Lehne, F. Preston, Making concrete change; innovation in low-carbon cement and concrete, Chatham House Rep. (2018) 1–122.
[13] S. Griffiths, B.K. Sovacool, D.D.F. DelRio, A.M. Foley, M.D. Bazilian, J. Kim, J. M. Uratani, Decarbonizing the cement and concrete industry: a systematic review of socio-technical systems, technological innovations, and policy options, Renew. Sustain. Energy Rev. 180 (2023), 113291.
[14] P.S. Fennell, S.J. Davis, A. Mohammed, Decarbonizing cement production, Joule 5 (2021) 1305–1311.
[15] V. Romanov, Y. Soong, C. Carney, G.E. Rush, B. Nielsen, W. O'Connor, Mineralization of carbon dioxide: a literature review, ChemBioEng Rev. 2 (2015) 231–256.
[16] S. Yadav, A. Mehra, A review on ex situ mineral carbonation, Environ. Sci. Pollut. Res. 28 (2021) 12202–12231.
[17] C.M. Woodall, N. McQueen, H. Pilorgé, J. Wilcox, Utilization of mineral carbonation products: current state and potential, Greenh. Gases: Sci. Technol. 9 (2019) 1096–1113.
[18] A. Sanna, M. Uibu, G. Caramanna, R. Kuusik, M. Maroto-Valer, A review of mineral carbonation technologies to sequester CO 2, Chem. Soc. Rev. 43 (2014) 8049–8080.
[19] A. Said, T. Laukkanen, M. Järvinen, Pilot-scale experimental work on carbon dioxide sequestration using steelmaking slag, Appl. Energy 177 (2016) 602–611.
[20] J. Tiefenthaler, L. Braune, C. Bauer, R. Sacchi, M. Mazzotti, Technological demonstration and life cycle assessment of a negative emission value chain in the Swiss concrete sector, Front. Clim. 3 (2021), 729259.
[21] ⟨http://www.neustark.com⟩, Accessed: 2023–03-11.2023.
[22] ⟨http://www.zirkulit.com⟩, Accessed: 2023–03-11.2023.
[23] R. Saran, V. Arora, S. Yadav, CO_2 sequestration by mineral carbonation: a review, Glob. NEST J. 20 (2018) 497–503.

[24] A. Azdarpour, M. Asadullah, E. Mohammadian, H. Hamidi, R. Junin, M.A. Karaei, A review on carbon dioxide mineral carbonation through pH-swing process, Chem. Eng. J. 279 (2015) 615–630.
[25] M. Meijssen, M. Mazzotti, Batchwise leaching of calcium from demolished concrete fines in an aqueous ammonium nitrate solution: part 1 experimental study, Ind. Eng. Chem. Res. 61 (2022) 15316–15325.
[26] J. Tiefenthaler, M. Mazzotti, Experimental investigation of a continuous reactor for CO_2 capture and CaCO3 precipitation, Front. Chem. Eng. (2022) 5.
[27] H. Jo, S.H. Park, Y.N. Jang, S.C. Chae, P.K. Lee, H.Y. Jo, Metal extraction and indirect mineral carbonation of waste cement material using ammonium salt solutions, Chem. Eng. J. 254 (2014) 313–323.
[28] M. Meijssen, M. Mazzotti, Batchwise leaching of calcium from demolished concrete fines in an aqueous ammonium nitrate solution: part 2 modeling, Ind. Eng. Chem. Res. 61 (2023) 15316–15325.
[29] U.R. Berner, Modelling the incongruent dissolution of hydrated cement minerals, Radiochim. Acta 44–45 (1988) 387–394.
[30] Y. Wang, Q. Yuan, D. Deng, Modelling calcium leaching kinetics of cement asphalt paste, Mater. Struct. /Mater. Et. Constr. (2018) 51.
[31] F.H. Heukamp, F.J. Ulm, J.T. Germaine, Mechanical properties of calcium-leached cement pastes: Triaxial stress states and the influence of the pore pressures, Cem. Concr. Res. 31 (2001) 767–774.
[32] B. Gérard, C. LeBellego, O. Bernard, Simplified modelling of calcium leaching of concrete in various environments, Mater. Struct. /Mater. Et. Constr. 35 (2002) 632–640.
[33] P. Derks, G. Versteeg, Kinetics of absorption of carbon dioxide in aqueous ammonia solutions, Energy Procedia 1 (2009) 1139–1146.
[34] S. Eloneva, P. Mannisto, A. Said, C.-J. Fogelholm, R. Zevenhoven, Ammonium salt-based steelmaking slag carbonation: precipitation of CaCO3 and ammonia losses assessment, Greenh. Gases: Sci. Technol. 1 (2011) 305–311.
[35] G. Wernet, C. Bauer, B. Steubing, J. Reinhard, E. Moreno-Ruiz, B. Weidema, The ecoinvent database version 3 (part I): overview and methodology, Int. J. Life Cycle Assess. 21 (2016) 1218–1230.
[36] Z. Kirova-Yordanova, Application of the exergy method to environmental impact estimation: the ammonium nitrate production as a case study, Energy 35 (2010) 3221–3229.
[37] Tschurtschenthaler, L., Gasós, A., Mazzotti, M. Experimental study of alternative reactor concepts for improved calcium extraction from demolished concrete fines; ETH Zurich, 2022; Master thesis.
[38] M. Zajac, J. Skocek, J. Skibsted, M.B. Haha, CO_2 mineralization of demolished concrete wastes into a supplementary cementitious material–a new CCU approach for the cement industry, RILEM Tech. Lett. 6 (2021) 53–60.
[39] B.J. Zhan, D.X. Xuan, C.S. Poon, K.L. Scrivener, Characterization of interfacial transition zone in concrete prepared with carbonated modeled recycled concrete aggregates, Cem. Concr. Res. 136 (2020), 106175.
[40] D. Rodríguez-Robles, P. Van den Heede, N. De Belie, New Trends in Eco-efficient and Recycled Concrete, Elsevier, 2019, pp. 207–256.
[41] Z. Zhao, S. Remond, D. Damidot, W. Xu, Influence of fine recycled concrete aggregates on the properties of mortars, Constr. Build. Mater. 81 (2015) 179–186.
[42] B. Klemczak, M. Batog, Heat of hydration of low-clinker cements: part I. Semi-adiabatic and isothermal tests at different temperature, J. Therm. Anal. Calorim. 123 (2016) 1351–1360.